

## THE FORMATION AND EVOLUTION OF STAR CLUSTERS IN INTERACTING GALAXIES

MOUPIYA MAJI<sup>1,2</sup>, QIRONG ZHU<sup>1,2</sup>, YUEXING LI<sup>1,2</sup>, JANE CHARLTON<sup>1</sup>, LARS HERNQUIST<sup>3</sup> AND ALEXANDER KNEBE<sup>4,5</sup>

<sup>1</sup>Department of Astronomy & Astrophysics, The Pennsylvania State University, 525 Davey Lab, University Park, PA 16802, USA

<sup>2</sup>Institute for Gravitation and the Cosmos, The Pennsylvania State University, University Park, PA 16802, USA

<sup>3</sup>Harvard-Smithsonian Center for Astrophysics, Harvard University, 60 Garden Street, Cambridge, MA, 02138, USA

<sup>4</sup>Departamento de Física Teórica, Módulo 8, Facultad de Ciencias, Universidad Autónoma de Madrid, E-28049 Madrid, Spain

<sup>5</sup>Astro-UAM, UAM, Unidad Asociada CSIC, E-28006 Madrid, Spain

### ABSTRACT

Observations of globular clusters show that they have universal lognormal mass functions with a characteristic peak at  $\sim 2 \times 10^5 M_\odot$ , but the origin of this peaked distribution is highly debated. Here we investigate the formation and evolution of star clusters in interacting galaxies using high-resolution hydrodynamical simulations performed with two different codes in order to mitigate numerical artifacts. We find that massive star clusters in the range of  $\sim 10^{5.5} - 10^{7.5} M_\odot$  form preferentially in the highly-shocked regions produced by galaxy interactions. The nascent cluster-forming clouds have high gas pressures in the range of  $P/k \sim 10^8 - 10^{12} \text{ K cm}^{-3}$ , which is  $\sim 10^4 - 10^8$  times higher than the typical pressure of the interstellar medium but consistent with recent observations of a pre-super star cluster cloud in the Antennae Galaxies. Furthermore, these massive star clusters have quasi-lognormal initial mass functions with a peak around  $\sim 10^6 M_\odot$ . The number of clusters declines with time due to destructive processes, but the shape and the peak of the mass functions do not change significantly during the course of galaxy collisions. Our results suggest that gas-rich galaxy mergers may provide a favorable environment for the formation of massive star clusters such as globular clusters, and that the lognormal mass functions and the unique peak may originate from the extreme high-pressure conditions of the birth clouds and may survive the dynamical evolution.

*Keywords:* galaxies: interactions, galaxies: star clusters: general, globular clusters: general, methods: numerical

### 1. INTRODUCTION

Star clusters (SCs) are building blocks of galaxies, so their origin and evolution are important aspects of the study of galaxy formation. Over the past two decades, numerous young massive clusters (YMCs) have been observed by the Hubble Space Telescope in interacting and merging galaxies, such as NGC 1275 (Holtzman et al. 1992), NGC 7252 (Whitmore et al. 1993), NGC 3921 (Schweizer et al. 1996), NGC 4038/39 or the Antennae Galaxies (Whitmore & Schweizer 1995; Whitmore et al. 1999, 2010), NGC 4449 (Annibali et al. 2011), and NGC 7176/7174 (Miah et al. 2015). The YMCs formed in these environments are compact ( $\sim$  few parsecs), gravitationally-bound objects with masses  $> 10^4 M_\odot$  and ages  $\sim 10 - 100$  Myr (Portegies Zwart et al. 2010). The initial cluster mass function (ICMF) of these young clusters, however, is not well-determined. Some studies suggested that it can be described as a

falling power law with  $dN/dM \propto M^{-2}$  (Zhang & Fall 1999; Bik et al. 2003; McCrady & Graham 2007; Fall & Chandar 2012), some argued that it might be better fit by a Schechter function with power index -2 and a characteristic mass of few  $10^6 M_\odot$  (Bastian 2008; Portegies Zwart et al. 2010), and some proposed that it is not a power law at all mass scales but has a turnover at the low mass end (Cresci et al. 2005; Anders et al. 2007).

On the other end of the SC spectrum are old globular clusters (GCs) that have been observed extensively in nearby galaxies (e.g., Harris 1991; Brodie & Strader 2006; Gratton et al. 2012; Kruijssen 2014, 2015). These are massive ( $\sim 10^4 - 10^6 M_\odot$ ), gravitationally-bound, compact (few pc) and old (age  $\simeq 10 - 13$  Gyr) systems that formed in the early universe and have survived to the present-day (Forbes & Bridges 2010; Vandenberg et al. 2013). It has been widely suggested that YMCs could be progenitors of these globular clusters (de Grijs 2007; Longmore et al. 2014). However, the observed globular cluster mass functions (GCMFs) are bell-shaped or lognormal-shaped with a peak mass

around  $1.5\text{--}3 \times 10^5 M_\odot$  (Harris 2001; Jordán et al. 2007), which are remarkably different from those of YMCs.

In order to explain the discrepancy between mass functions of YMCs and GCs, a number of studies have focused on the dynamical evolution of SCs. Some theorized that the GCs were formed from the collapse of protogalactic clouds and these clusters had bell shaped ICMFs to begin with (Fall & Rees 1985; Vesperini 2000, 2001; Parmentier & Gilmore 2007). The more prevalent theory suggested that young GCs start with a power-law ICMF, and during evolution they are affected by a number of destructive processes that can disrupt the lower mass clusters more easily and more frequently than their higher mass counterparts, resulting in a lognormal profile (Gnedin & Ostriker 1997; Baumgardt 1998; Fall & Zhang 2001). Such destruction can rise from two-body relaxation, shock heating, supernova explosions, tidal shocking and stellar dynamical evaporation (e.g., Gnedin et al. 1999a; Fall & Zhang 2001; McLaughlin & Fall 2008). In particular, tidal forces induced by galaxy interactions or GCs passing through a galactic disk can generate efficient heating from massive tidal shocks, which significantly affect the evolution of GCs (Combes et al. 1999; Gnedin et al. 1999a,b).

However, little is known about the formation conditions that determine the mass functions of YMCs and how they are related to those of GCs. It has long been suggested that globular clusters preferentially form in regions with extremely high pressure (Elmegreen & Efremov 1997; Ashman & Zepf 2001). High pressure in molecular clouds can result in high velocity dispersions (several tens of km/s) which lead to larger binding energy. This helps the cloud not to get dispersed by typical HI clouds. With rising pressure, the specific star formation efficiency of the region can increase significantly by up to one order of magnitude (Jog & Solomon 1992; Jog & Das 1996). High binding energy and high specific star formation efficiency are critical to the formation of massive, bound SCs. From the present-day properties of GCs, it is suggested that the cluster-forming clouds should have experienced high pressure on the order of  $P/k_B \gtrsim 10^8 \text{ K cm}^{-3}$ , which is  $\gtrsim 10^4$  times larger than the ambient interstellar medium pressure in our galaxy (Jenkins et al. 1983; Boulares & Cox 1990; Elmegreen & Efremov 1997; Welty et al. 2016). However, these extreme pressures can be easily produced in interacting galaxies by violent shocks, so they are theoretically expected to be ideal formation sites for GCs.

On the observational front, it has been difficult to directly observe the physical conditions of a proto super-star cluster cloud (SSC - star clusters with the possibility of evolving into GCs). Wei et al. (2012) observed molecular cloud regions in the Antennae Galaxies and found very massive ( $\gtrsim 10^6 M_\odot$ ) clouds in the centers of

high star formation regions with large velocity dispersion. Recently, Johnson et al. (2015) have studied the properties of a pre-SSC cloud in the merging galaxies of the Antennae in detail via CO observations. This cloud is not yet forming stars, but is expected to begin doing so in less than 1 Myr, which makes it an ideal candidate to investigate SSC formation conditions. Direct measurements of the cloud suggest that it has mass of  $> 5 \times 10^6 M_\odot$  and a radius of  $\sim 25 \text{ pc}$  which falls in the range of GC properties. The cloud is experiencing a tremendously high external pressure  $P/k_B > 10^8 \text{ K cm}^{-3}$ . Adamo et al. (2015) studied the SCs in M83 at different radii from the galaxy center and concluded that high gas pressure increases cluster formation efficiency.

In order to investigate the formation and evolution of SCs and their mass functions, we need realistic simulations of galaxies with SC systems to understand the complex interplay of all the creation and destruction processes. However, due to the large dynamical range (from sub pc for star formation to kpcs for galaxies), mass scale (from star clusters of  $\sim 10^4 M_\odot$  to galaxies of  $10^{12} M_\odot$ ), and the various physical processes involved (cluster formation in GMCs, stellar evolution, binary interaction, shocks, tidal disruptions etc), it has been a challenge to study formation and evolution of SCs in galaxies numerically. Most of the early simulation efforts assumed a shape for the ICMF of clusters, generally power laws or Schechter functions, and then simulated their evolution using N-body codes (Vesperini & Heggie 1997; Baumgardt & Makino 2003; Lamers et al. 2010). Some simulations have focused on particular aspects of the problem, such as the evolution of GCs in the tidal fields of mergers (Renaud & Gieles 2013), star escape rate from GCs (Gieles & Baumgardt 2008) and the effects of intermediate mass black holes on GCs (Lützgendorf et al. 2013). A few simulations explore SCs in specific environments such as high redshift galaxies (Prieto & Gnedin 2008) and dwarf galaxies (Kruijssen & Cooper 2012). Some variants of N-body simulations have also been applied, for example, Renaud et al. (2011) used a tensor field to describe tidal fields.

It is very important to include hydrodynamics of the gas in the galaxy to fully understand SC formation and evolution, but it can be highly computationally expensive to explore the entire range of processes. For example, Li et al. (2004) used sink particles to represent SCs in high-resolution, smoothed particle hydrodynamics (SPH) simulations but could not follow the structure of clusters; Kruijssen et al. (2011, 2012) used N-body/hydro simulations for the galaxies but followed the cluster evolution semi-analytically. A more complete treatment of galaxy simulation and SC identification emerged recently. Renaud et al. (2015) modeled an Antennae-like merger using an adaptive mesh refine-

ment (AMR) grid-based code and identified SCs with a friends-of-friends (FOF) group finding algorithm. They found that the cluster formation rate roughly follows the star formation rate, and that clusters formed in interacting galaxies are up to 30 times more massive than those formed in isolated galaxies. However, a detailed study of the formation conditions of SCs and the evolution of cluster mass functions is needed.

In this study, we perform fully hydrodynamic simulations of galaxy mergers using two different codes: GADGET (Springel et al. 2001; Springel 2005) and GIZMO (Hopkins 2015). We identify the SCs in them as overdense groups of bound particles, using the Amiga Halo Finder (AHF<sup>1</sup>, Gill et al. 2004; Knollmann & Knebe 2009). We investigate the physical conditions of SC formation by tracking the properties of the nascent birth clouds. We follow the early evolution of their mass function to understand the connection between YMCs and GCs and the origin of the mass function peak of GCs. This is one of the first studies to realistically identify SCs and follow their formation and evolution in galaxy mergers.

Our paper is organized as follows: in § 2 we describe the methods, which include the numerical codes, galaxy model and cluster identification; in § 3 we present the results of cluster formation and physical conditions, and the initial cluster mass functions; in § 4 we explore the evolution of cluster mass functions; in § 5 we discuss the limitations of our study; and we summarize our findings in § 6.

## 2. METHOD

In this study, we perform hydrodynamical simulations of a galaxy merger of two Milky Way-size progenitors using two different hydrodynamics codes: the improved SPH code GADGET developed by Springel et al. (2001) and Springel (2005), and the new meshless code GIZMO developed by Hopkins (2015). In order to reduce numerical artifacts on the physical results, we have implemented the same physical processes in both codes, and use the same initial conditions in the simulations. The SCs are identified in the simulations using a density-based group finding algorithm Amiga Halo Finder (AHF, Knollmann & Knebe 2009; Gill et al. 2004). In what follows we briefly describe the codes, galaxy model and SC identification used in the simulations; we refer the reader to read the references therein for detailed descriptions.

### 2.1. Hydrodynamic Codes

GADGET (Springel et al. 2001; Springel 2005) is a massively parallel N-body/SPH code. It handles the components of a galaxy in two distinct ways: it treats the motions and evolution of dark matter and stars as collisionless particles in an N-body problem, while the gas is dealt with using the SPH method (Gingold & Monaghan 1977; Hernquist & Katz 1989). The N-body particles are described by the collisionless Boltzman and Poisson equations, and the hydrodynamics of the fluid is followed using properties of neighboring gas particles smoothed by a kernel function. The gravitational force of each particle is calculated with a tree algorithm in which particles are grouped together and their effect is taken as a single multipole force, which reduces the computation cost greatly to  $O(\log N)$  compared to the direct summation of each particle pair with complexity  $O(N)$ . In this code, an artificial viscosity term is introduced into the equation of motion of SPH to represent the viscosity which often arises in ideal gases due to shocks caused by microphysics. The GADGET-2 we use explicitly conserves energy and entropy in the SPH formulation (Springel & Hernquist 2002). This version and its variants have been widely used in a large number of applications, from large-scale cosmological simulations (e.g., Springel & Hernquist 2003b; Springel et al. 2005b; Feng et al. 2013; Schaye et al. 2015) to galaxy mergers (e.g., Springel 2000; Li et al. 2004; Springel & Hernquist 2005; Hopkins et al. 2005, 2006, 2008; Li et al. 2007; Cox & Loeb 2008; Hayward et al. 2014).

GIZMO (Hopkins 2015) is a new Lagrangian code developed to circumvent the many problems encountered by SPH methods (Agertz et al. 2007; Bauer & Springel 2012; Vogelsberger et al. 2012; Sijacki et al. 2012; Kereš et al. 2012; Nelson et al. 2013; Zhu et al. 2015; Zhu & Li 2016). It derives the hydrodynamic equations using a kernel function to partition the volume, and a Riemann solver to evolve the equations at the Lagrangian face comoving with the mass. GIZMO implements strict conservation of mass, energy and linear and angular momentum and it does not require any artificial diffusion terms to deal with shocks, embodying the advantages of both SPH and grid-based methods. It captures the instabilities of fluid mixing well, greatly reduces numerical noise and artificial viscosity and as a result calculates fluid physics at smaller Mach number more accurately. GIZMO treats the contact discontinuities and shocks more precisely and more efficiently, generally within one kernel length instead of 2-3 as in GADGET, and it does not have the zeroth order and first order errors that are present in SPH (Zhu et al. 2015), so it can attain higher accuracy with a much smaller number of neighbors which results in a faster convergence. We have used the meshless finite-mass mode of Gizmo for our project. The mass of an individual gas element is conserved in this

<sup>1</sup> The AHF code is available at <http://popia.ft.uam.es/AHF/Download.html>

mode, which allows us to trivially trace the history of star particles to their progenitor gas particles (otherwise, one needs tracer particles to do so).

A detailed comparison between GADGET and GIZMO in galaxy simulations has been conducted by [Zhu & Li \(2016\)](#), who showed a general agreement between the two simulations but there were notable differences in a number of galaxy properties such as star formation history, gas fraction and disk structures.

In this study, our motivation for using these two codes to perform the same merger simulation is to effectively rule out the possibility of numerical artifacts in our results. As we will show in § 3, although the detailed star formation history of the mergers is different between the two simulations, the overall distribution functions of the cluster mass and the pre-cluster gas pressure agree well, which suggests that our results are physical and robust, because we can argue against the effects of numerical artifacts such as the number of neighbors and artificial viscosity on these results.

## 2.2. Galaxy Model

Our simulations consider major mergers of two equal-mass Milky Way - sized galaxies. The galaxy is constructed using the model of [Mo et al. \(1998\)](#), which has a dark matter halo with a Hernquist density profile ([Hernquist 1990](#)), a thin disk with gas and stars, and a black hole in the center. The galaxy properties are similar to those of the Milky Way: the total mass is  $10^{12} M_{\odot}$ , the gas fraction  $f_{\text{gas}} = 0.2$ , the disk height is one-fifth of the radial scale length of the galaxy, the disk contains 4% of its total mass, and the seed mass of the black hole is  $10^5 M_{\odot}$ .

The interstellar medium (ISM) in these galaxies is modeled using a sub-grid multi-phase recipe, and the star formation rate follows the empirical Schmidt-Kennicutt law ([Schmidt 1959](#); [Kennicutt 1998](#)) where the surface density of star formation is related to the surface density of gas ( $\Sigma_{\text{SFR}} \propto \Sigma_{\text{gas}}^{1.4}$ ). The radiative cooling and heating in the ISM is modeled with the assumption that the medium is in collisional equilibrium and there is an external UV background ([Haardt & Madau 1996](#)). We have also followed feedback processes from both supernovae ([Springel & Hernquist 2003a](#)) and active galactic nuclei ([Springel et al. 2005a](#)). Supernova feedback includes thermal energy and galactic winds. The wind energy efficiency is 5% of the supernovae energy, and the wind direction is anisotropic: winds carry energy and matter perpendicular to the disk plane. The feedback from the black holes is in the form of thermal energy deposited isotropically into the surrounding gas.

We note that [Renaud et al. \(2015\)](#) have performed a simulation of Antennae-like merger. In order to explore a more extreme merger environment, we simulate a

nearly head-on collision of two Milky Way-sized galaxies. In the simulations, each galaxy is initially started with 82,000 gas particles, 328,000 star particles and 1,476,860 dark matter particles, which yield a mass resolution of  $5 \times 10^4 M_{\odot}$  for the gas and star particles, and  $6 \times 10^5 M_{\odot}$  for each dark matter particle.

## 2.3. Star Cluster Identification

Finding groups or structures in a given set of data is a classic problem in data mining. There are many algorithms for group finding, which essentially differ in their notion of groups and in their methods. The two main classes are particle-based and density-based algorithms. The most widely used method of group finding in astronomy is the FOF algorithm ([Davis et al. 1985](#)). It is a particle-based algorithm where all particles within a given linking length are considered as a group. However, there are two significant downsides of this approach even with an adaptive linking length ([Suginohara & Suto 1992](#)): i) if two groups have a linking bridge, they will be identified as one group; ii) it cannot identify substructures within a structure.

The other class of group-finding algorithms is density-based, which identify overdensities in the field as groups ([Warren et al. 1992](#); [Bertschinger & Gelb 1991](#); [Klypin & Holtzman 1997](#); [Gill et al. 2004](#)). These methods do not suffer from the problems of the FOF methods described above. For this reason, we adopt the density-based hierarchical group finding algorithm AHF ([Knollmann & Knebe 2009](#)) to identify SCs in the simulations using the following procedures.

First, AHF divides the simulation box into grid regions. It determines the density inside each grid cell and compares the density to a threshold or background density value. If the computed density exceeds the threshold, it divides the grid into half of its initial size. It computes the densities in each of the refined grid cells and again compares with the threshold. This process goes on recursively until all the cells in the simulation box have densities less than the threshold value. Next, it starts from the finest grid and marks isolated overdense regions as possible clusters. It goes on to the next coarser level and again identifies possible regions as clusters. Importantly, it links the possible clusters in finer grids to their respective coarser parts (linking daughters to parents). This continues until it has reached the coarsest grid and finally it builds a tree of clusters with subclusters.

Considering the observed physical properties of young massive clusters, we impose a few conditions on the groups found by AHF to qualify them as SCs. We require at least 4 particles to form a cluster which means the minimum cluster mass is  $2 \times 10^5 M_{\odot}$ . The group has to be gravitationally bound, has stars,

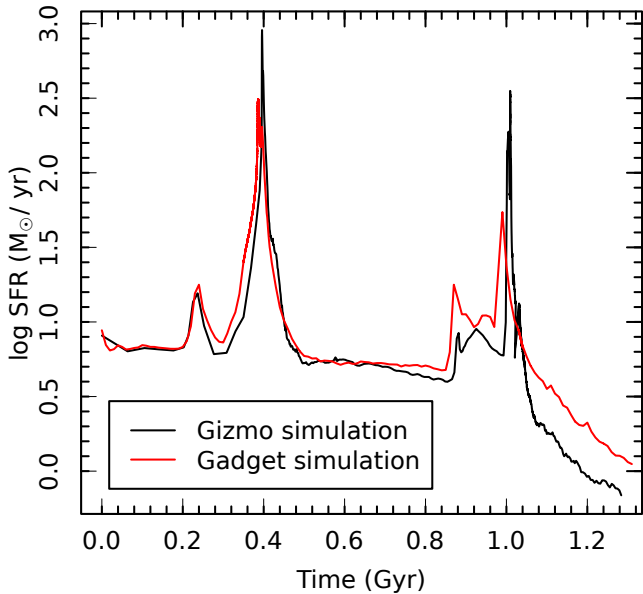


**Figure 1.** The star formation histories of galaxy mergers in both GIZMO (black curve) and GADGET (red curve) simulations. The peaks in star formation occur during the close encounters of the progenitors (Mihos & Hernquist 1994, 1996).

contains no substructures and has a baryonic fraction  $f_b = \text{baryon mass}/\text{dark matter mass} > 1$ . The upper limit of mass is set at  $10^8 M_\odot$ . Such an approach provides a holistic identification of star clusters in our study.

### 3. FORMATION OF STAR CLUSTERS

#### 3.1. Starbursts in Interacting Galaxies

In the simulations, the progenitor galaxies start moving towards each other at  $t = 0$  on a parabolic orbit. They have their first close encounter at  $t \sim 0.25$  Gyr, and the second one at  $t \sim 0.9$  Gyr until the final coalesce at  $t \sim 1$  Gyr. During the close passages, vigorous star formation is triggered by the compression of gas by tidal forces and rising gas densities in the inner region of the galaxies due to gravitational torques (Barnes & Hernquist 1991, 1996). As shown in Figure 1, the first starburst occurs at  $t \sim 0.2 - 0.5$  Gyr, when the star formation rate (SFR) increases by nearly two orders of magnitude and reaches a peak of  $\sim 10^3 M_\odot/\text{yr}$  at  $t \sim 0.4$  Gyr. The second starburst takes place at  $t \sim 0.9 - 1.1$  Gyr, and the SFR peaks at  $\sim 10^2 M_\odot/\text{yr}$  at  $t \sim 1$  Gyr.

We note a remarkable difference in the star formation histories between the two simulations in that GIZMO produces higher SFR peaks than GADGET by a factor of 3 – 5. This is due to the more accurate treatments of fluids and shocks in GIZMO. Similar differences have also been seen in the code comparison study of galaxy merg-

ers using GADGET and the moving-mesh code AREPO by Hayward et al. (2014), who reported that AREPO produces higher SFRs than GADGET by up to a factor of 10 for mergers of Milky Way - size galaxies. In the simulation of Antennae mergers, Renaud et al. (2015) reported a peak SFR of  $\sim 10^2 M_\odot$ , which is lower than ours due to smaller progenitors and different orbital parameters in their simulation.

The strong compression and shocks produced by the galaxy interaction fuel rapid formation of SCs during the starbursts. As demonstrated in Figure 2, most of the SCs form in the nuclear regions of the two merging galaxies, with a few spread in the tidal tails and the galactic bridges. Similar distributions of YMCs have also been observed in galaxy mergers, including nuclear region clusters by Whitmore & Schweizer (1995); Miller et al. (1997), and tidal tail clusters by Barnes & Hernquist (1992); Knierman et al. (2003); Bastian et al. (2005); Mullan et al. (2011).

#### 3.2. Initial Cluster Mass Functions

The resulting mass functions of the SCs formed during the first close encounter are shown in Figure 3. Although the total number of clusters in the same snapshot differs between the GIZMO and GADGET simulations by a factor of  $\sim 1.3$ , the range of  $\sim 150 - 200$  is in good agreement with observations of galaxy mergers such as the Antennae (Whitmore et al. 1999; Larsen 2010). More interestingly, both simulations produce similar mass distributions which resemble a peaked or a quasi-lognormal function, with a GIZMO peak around  $10^{5.8-6} M_\odot$  and the GADGET peak at  $10^{6-6.2} M_\odot$ .

Our mass functions do not show a purely declining power law, as suggested by many observations of YMCs (e.g., Zhang & Fall 1999; Bik et al. 2003; McCrady & Graham 2007; Fall & Chandar 2012). This could be due to our limited resolution at the low mass end ( $5 \times 10^4 M_\odot$ ), which prevents the simulation from forming and identifying low mass clusters. However, Renaud et al. (2015) also reported lognormal-shape ICMFs from their Antennae simulation even though they have a much higher mass resolution ( $\sim 70 M_\odot$ ). It is also possible that the power-law phase is extremely short lived ( $< 10$  Myr) in violent mergers and our snapshot interval (every 10 Myr) misses that phase. We note, however, some observations have suggested that the power law ICMF for YMCs is not universal, rather they have a turnover at low mass (Cresci et al. 2005; Anders et al. 2007).

The peak masses of these ICMFs are higher than those of the observed GCMFs,  $\sim 1.5 - 3 \times 10^5 M_\odot$ , but it can be predicted that after an evolution of Gyrs, stellar evolution, tidal stripping and other disruptive processes will cause them to lose some of their mass (Kruijssen 2015;

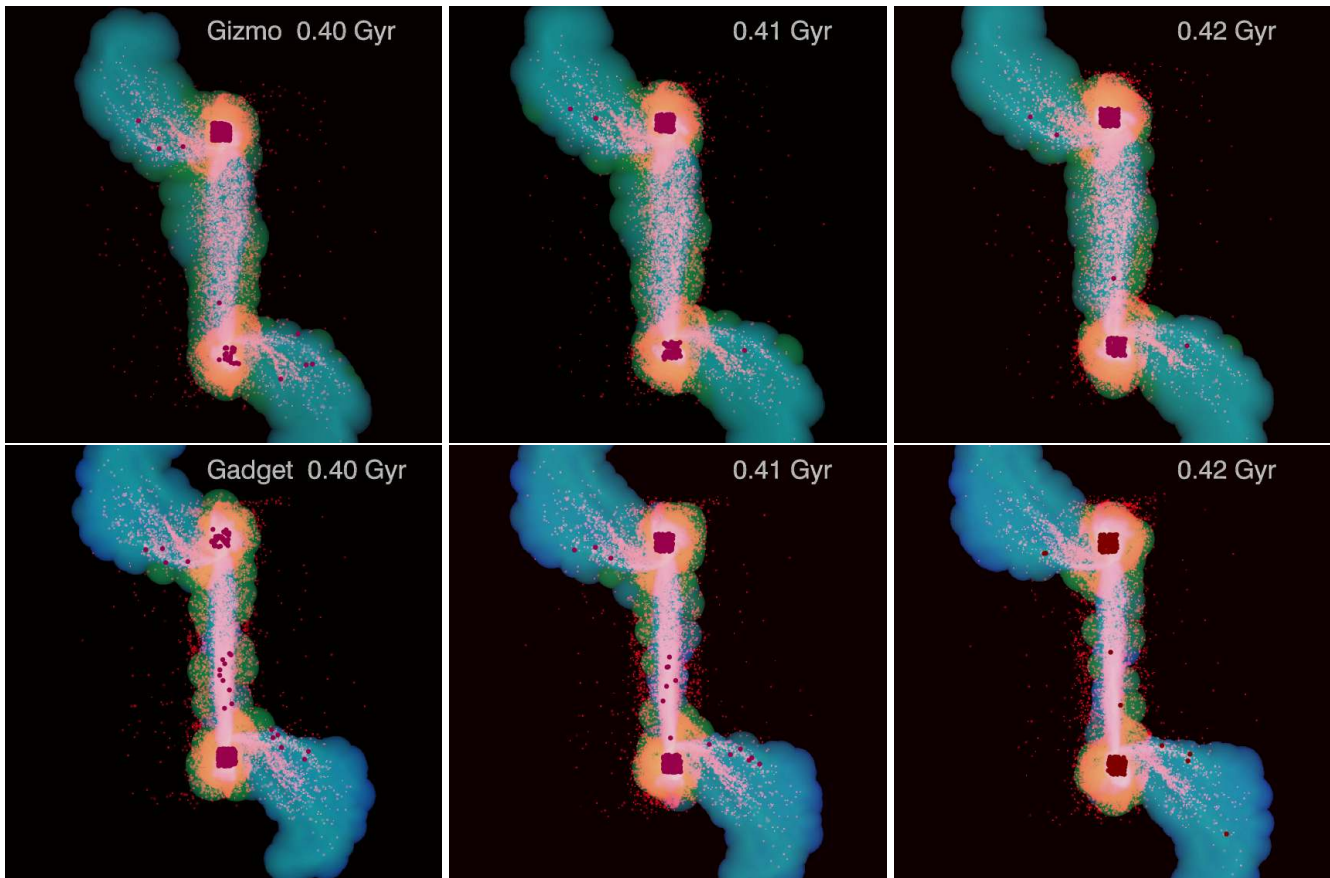


**Figure 2.** Snapshots of the galaxy merger at three different times, 0.40 Gyr, 0.41 Gyr and 0.42 Gyr during the first starburst phase when most clusters form, from both GIZMO (top panels) and GADGET (bottom panels) simulations. The images are projected gas density maps color-coded by gas temperature (the colors from blue to red indicates hotter gas, the brightness from dark to white measures increasing density). The red dots are stars, and the filled maroon circles represent nearly formed star clusters. The maroon region in the center of each galaxy indicates overlapping star clusters. The box length is 100 kpc in physical coordinates.

Webb & Leigh 2015). We discuss their evolution in more detail in §4. It is encouraging that both of our simulations, together with that by Renaud et al. (2015), produce similar quasi-lognormal ICMFs with similar peak positions, despite having vastly different hydrodynamic solvers, feedback processes and numerical resolutions. This agreement suggests that the lognormal mass function is unlikely due to numerical artifacts but has a physical origin, which will be investigated in the next section.

### 3.3. Physical Conditions of Cluster Formation and Origin of Lognormal Cluster Mass Functions

In order to explore the physical origin of the quasi-lognormal ICMFs in Figure 3, we examine the physical conditions of cluster formation. As mentioned in § 1, massive SCs form in molecular clouds with very high gas pressures (Elmegreen & Efremov 1997; Ashman & Zepf 2001). When a star-forming cloud is under high pressure, the efficiency of star formation increases and the gas velocity dispersion becomes higher, which in turn help to keep the cloud bound (Jog & Solomon

1992). These physical conditions create an ideal nursery to form massive, gravitationally-bound clusters. Recently, Zubovas et al. (2014) performed an N-body simulation of a molecular cloud and concluded that high external pressures drive efficient star formation and can cause cloud fragmentation, leading to the formation of star clusters. Quantitatively, the external pressure  $P$  on a nascent molecular cloud is given by Elmegreen (1989):

$$P = \frac{3\Pi M_{\text{cloud}}\sigma_v^2}{4\pi r^3} \quad (1)$$

where  $M_{\text{cloud}}$  is the mass of the cloud,  $\sigma_v$  is the velocity dispersion and  $r$  is the size of the cloud. The factor  $\Pi$  is given by the ratio of density at the cloud edge and the average density,  $\Pi = n_e/\langle n_e \rangle$  and is generally approximated to be 0.5.

We can calculate the approximate cloud pressure of GC progenitors using their present day properties. For a virialized cluster the pressure given by Equation 1 can be expressed as  $P \sim \rho\sigma_v^2 \sim G\sigma^2$ , where  $G$  is gravitational constant and  $\sigma$  is the mass column density. For a

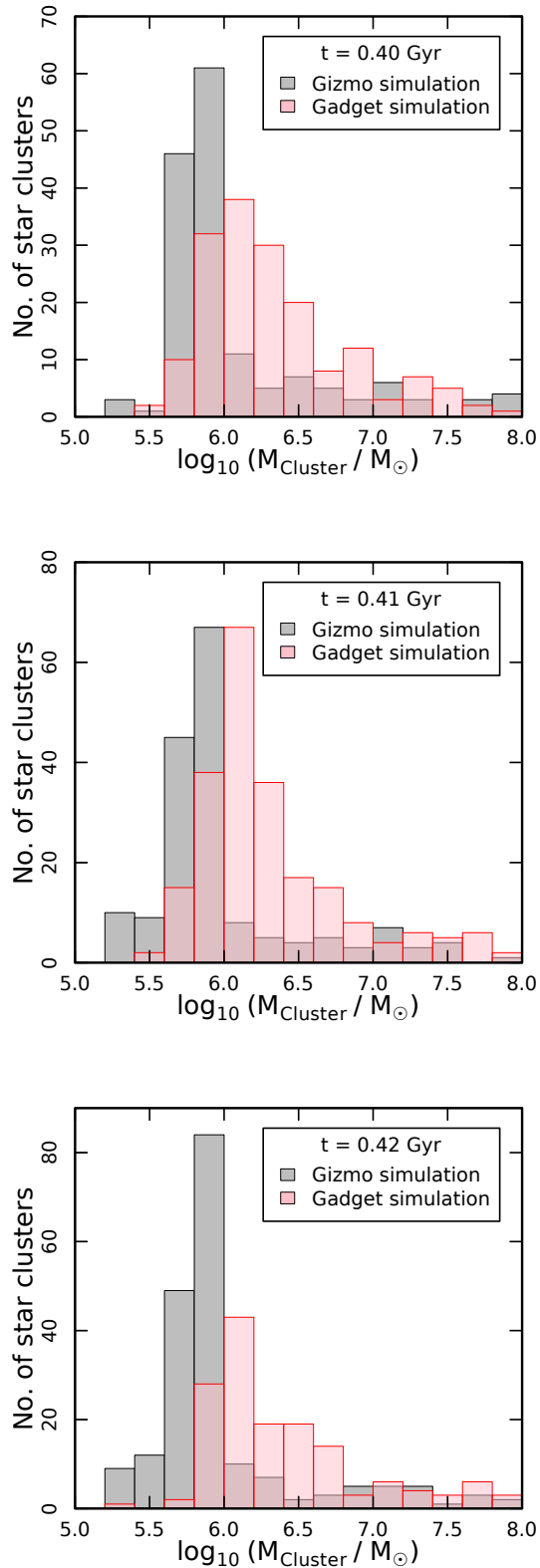


**Figure 3.** Mass functions of star clusters formed at 0.40 Gyr, 0.41 Gyr and 0.42 Gyr during the first starburst phase when most clusters form, from both GIZMO (grey) and GADGET (red) simulations. The total number of clusters in the three snapshots from GIZMO (GADGET) simulation is 158 (170), 171 (221), and 197 (151), respectively.

globular cluster with mass  $10^6 M_\odot$  and radius 10 pc, the pressure of this GC is  $P/k_B \sim 10^8 \text{ Kcm}^{-3}$  which is  $\gtrsim 10^4$  times higher than the ISM pressure in the Milky Way (Jenkins et al. 1983; Boulares & Cox 1990; Welty et al. 2016). The pressure in the birth clouds of GC progenitors or SSCs is therefore expected to be  $\gtrsim 10^8 \text{ Kcm}^{-3}$  (Elmegreen & Efremov 1997).

In the simulations, in order to determine the pressure of the clouds from which the SCs form, we track the cluster members back in time. We take the constituent star particles of a cluster and identify the gas particles from which they formed. We then measure the velocity dispersion of these gas particles and approximate the gas cloud radius as the average distance from gas particles to the center of mass of the cloud. With these parameters, we can then calculate the cloud pressure using Equation 1. In Figure 4, we show the resulting pressure distributions against the cluster mass distributions, in comparison with the pressure of a pre-SSC cloud observed in the Antennae by Johnson et al. (2015). We also calculate the pressures of observed SCs in the Antennae Galaxies using the velocity and radius data compiled in Portegies Zwart et al. (2010) and Mengel et al. (2002, 2008) for comparison.

As shown in Figure 4, the pre-cluster cloud pressures from both the GIZMO and GADGET simulations fall in the range of  $P/k \sim 10^8 - 10^{12} \text{ Kcm}^{-3}$ , in good agreement with observations of a proto-SSC cloud in Antennae (Johnson et al. 2015), but they are  $10^4 - 10^8$  times higher than the typical pressure in the ISM (Jenkins et al. 1983; Boulares & Cox 1990; Welty et al. 2016). Our results support the theoretical expectations that massive SCs form in high-pressure clouds.

Moreover, the pressure distributions have near lognormal-shape profiles in all panels. Such a quasi lognormal-shape pressure distribution may be the cause of the quasi lognormal-shape ICMF. If we assume a certain cluster formation efficiency  $\eta$  ( $\eta$  that varies with galactic environment, from 0.01 in quiescent galaxies to  $> 0.4$  in interacting galaxies, as suggested by Goddard et al. 2010; Kruijssen 2015), then the mass of a SC  $M_{\text{cluster}}$  may be related to that of the birth clouds  $M_{\text{cloud}}$  as  $M_{\text{cluster}} \propto \eta M_{\text{cloud}}$ ; then by inverting Equation 1 we get  $M_{\text{cluster}} \propto \eta M_{\text{cloud}} \propto \eta P$ . This qualitative relation, as can be inferred from Figure 4, suggests that the distribution of cluster mass depends on that of the cloud pressure, so a lognormal pressure distribution may lead to a lognormal mass distribution of the resulting clusters.

Furthermore, Figure 4 also shows that the pressure profiles have a peak at cluster mass around  $10^{5.8-6} M_\odot$  in the GIZMO simulation and around  $10^{6-6.2} M_\odot$  in the GADGET simulation, which are exactly the same peaks of their corresponding mass functions. This striking corre-

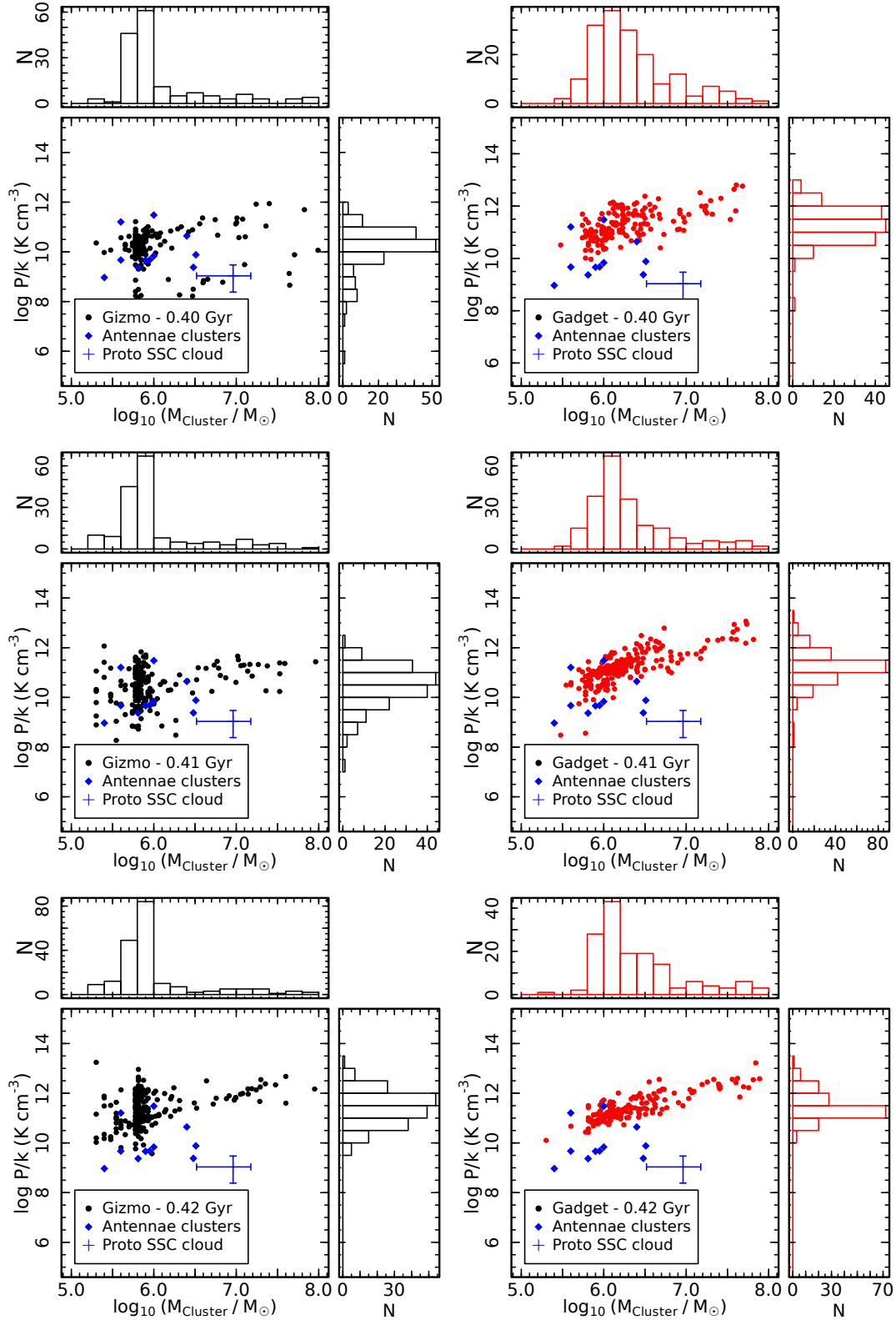


**Figure 4.** Correlation between pre-cluster gas pressure distributions and initial cluster mass functions at 0.40 Gyr, 0.41 Gyr and 0.42 Gyr during the first starburst phase, when most clusters form, from both GIZMO (black) and GADGET (red) simulations. The pressure derived from the observed pre-super star cluster cloud in the Antennae by [Johnson et al. \(2015\)](#) is represented by the blue cross where the error bars reflect the observational uncertainties in cloud mass ( $3.3 - 15 \times 10^6 M_{\odot}$ ), radius ( $24 \pm 3$  pc) and velocity dispersion ( $49 \pm 3$  km/s). The pressures derived from observed star clusters in the Antennae using velocity and radius data compiled in [Portegies Zwart et al. \(2010\)](#) and presented by [Mengel et al. \(2002, 2008\)](#) are represented by blue diamonds. The pressure is expressed as  $P/k$  where  $k$  is the Boltzman constant.



lation may explain the preferred mass range around the characteristic peak  $10^6 M_\odot$ , as determined by the cloud pressure, for the newly formed SCs in galaxy mergers.

The major source of rising pressure in interacting galaxies is shocks. When two galaxies merge, the neutral hydrogen clouds collide with each other with high relative velocity and they create a hot and ionized gas remnant. This gas plasma can exert tremendous radiative shock compression on the giant molecular clouds in the galaxy, which leads to an increase in the cloud pressure (Jog & Solomon 1992; Ashman & Zepf 2001). Recent observations of the Antennae by Zhang et al. (2010) found that the SFR is much higher in the overlapping regions of the two progenitors compared to other regions, which supports the theory of shock-induced star formation. Studies of molecular clouds in the Antennae revealed very high velocity dispersion in high star-forming regions, which can also be explained by compressive shocks (Wei et al. 2012). In addition, Herrera et al. (2011) carried out near infrared imaging spectroscopy of the same region and found extended line widths in  $H_2$  emission, which indicates powerful shocks in the region. Keto et al. (2005) studied the CO emission of the starbursting merger of M81 /M82, and found that the molecular clouds undergoing star formation are driven by shock compression.

We can see from Figure 4 that the pressures of our simulated clouds are somewhat higher than that of the observed systems. This can arise from the fact that in our simulation the two equal-mass, Milky Way - size galaxies collide mainly head on and merge violently, whereas the Antennae Galaxies have a smaller mass and they are on a milder pericentric passage (Renaud et al. 2015). The extreme conditions in the simulated galaxies produce more powerful shocks which in turn help increase the gas pressure. Such an extreme high-pressure environment may preferentially form massive SCs in a narrow mass range as shown in Figure 3, which may help to explain why we do not see a power-law ICMF in the simulations.

Our simulations bridge the observations and theories of cluster formation and we confirm that massive SCs can form in gas-rich galaxy mergers due to the high gas pressure produced by strong gravitational interactions. Moreover, the special pressure range in such merger environments preferentially forms SCs in a narrow mass interval around the peak mass at  $\sim 10^6 M_\odot$ . Furthermore, the quasi-lognormal pressure distribution may lead to the quasi-lognormal ICMF of SCs formed in colliding galaxies. Our results, therefore, provide clues to the formation of globular clusters and their universal log-normal mass functions, which will be explored in the next section.

#### 4. EVOLUTION OF MASSIVE STAR CLUSTERS

In order to track the change of the cluster mass functions over time, we follow the evolution of the massive SCs in our simulations up to 1.3 Gyr when the progenitors completely coalesce. After the initial bursts of star and SC formation during the first close passage at  $t \sim 0.2-0.5$  Gyr, the activity decreases, and many of the clusters are destroyed over time. However, the starburst activity is renewed again at  $t \sim 0.9-1.1$  Gyr during the final coalescence, although at a lower amplitude than the first burst.

Figure 5 shows the probability density function (PDF) of the cluster mass distribution at different times from both GIZMO and GADGET simulations. Interestingly, the PDFs from the GIZMO simulation have similar narrow profiles, and the position of the peak remains nearly the same over 1 Gyr, while those from the GADGET simulation show a slow evolution from a broad profile to a narrow one and a shift of the peak mass by 0.3 dex over 1 Gyr. The narrowing of the PDF is due to destruction of SCs at both low- and high-mass end by a variety of processes, such as tidal and shock heating, two-body interactions, and supernovae explosions (Gnedin et al. 1999a; Fall & Zhang 2001; McLaughlin & Fall 2008) which are included in the hydrodynamic simulations. After  $\sim 1$  Gyr of evolution, about one fourth of the SCs are left, most of them just around the peak mass. The difference in the narrowness of the PDFs from the two simulations is also present in their initial mass functions in Figure 3. This probably stems from the different pressure distributions (Figure 4) owing to different treatments of shocks between GIZMO and GADGET, as discussed in § 2.1.

The peak for each density curve is the value of the most probable mass of the clusters for that time, as shown in Figure 6. The most probable cluster mass in the GIZMO simulation is remarkably consistent at  $\sim 10^{5.8} M_\odot$  over 1 Gyr, while that of the GADGET simulation changes slightly from  $\sim 10^{6.09} M_\odot$  at the initial starburst to  $\sim 10^{5.8} M_\odot$  after 1 Gyr. Since these are isolated merger simulations, it is meaningless to continue the simulations for a longer time, but in a cosmological context, it can be predicted that the SCs will lose some of their mass due to stellar evolution and other destructive processes. Semi-analytical and N-body simulations by Kruijssen (2015) and Webb & Leigh (2015) found that clusters can lose mass by a factor of 2 – 4 after a Hubble time of evolution. The eventual mass of our simulated clusters can be similar to the observed peak mass of globular clusters at  $1.5 - 3 \times 10^5 M_\odot$  (Harris 2001; Jordán et al. 2007).

These two figures show that both the shape of the mass function and the position of the mass peak have little evolution over the course of the galaxy collision

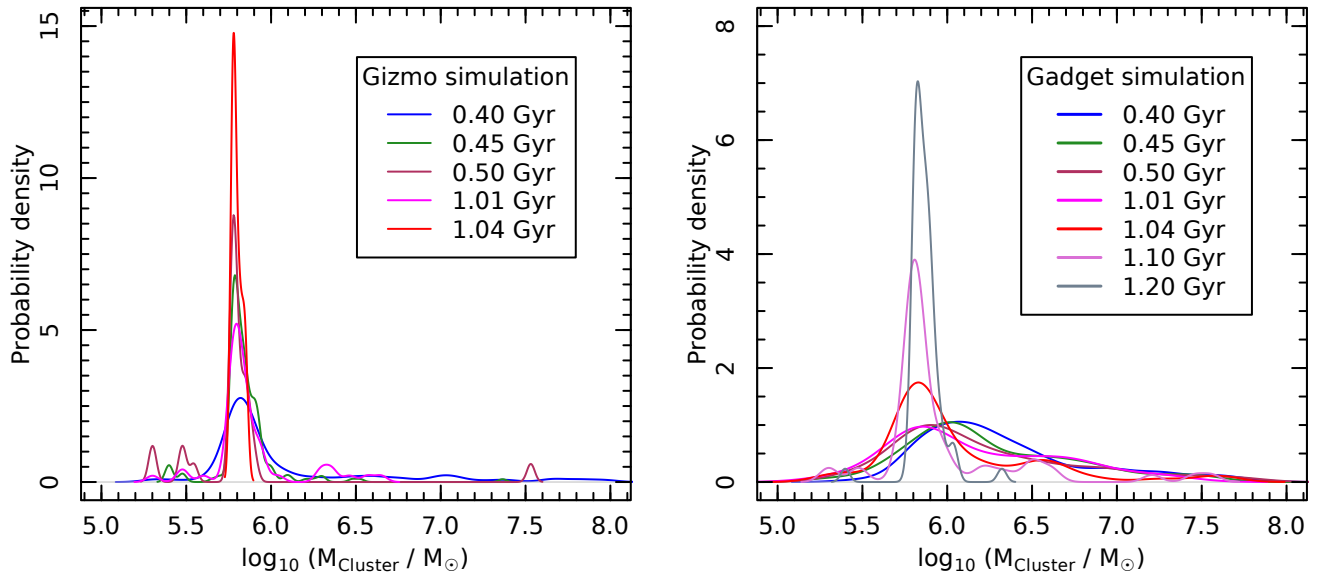


**Figure 5.** Probability density function of star cluster mass distribution from both GIZMO (left panel) and GADGET (right panel) simulations at different times, as indicated by the different colors. A Gaussian profile is used as the kernel density estimator. The PDFs are normalized such that the area under each curve is unity.

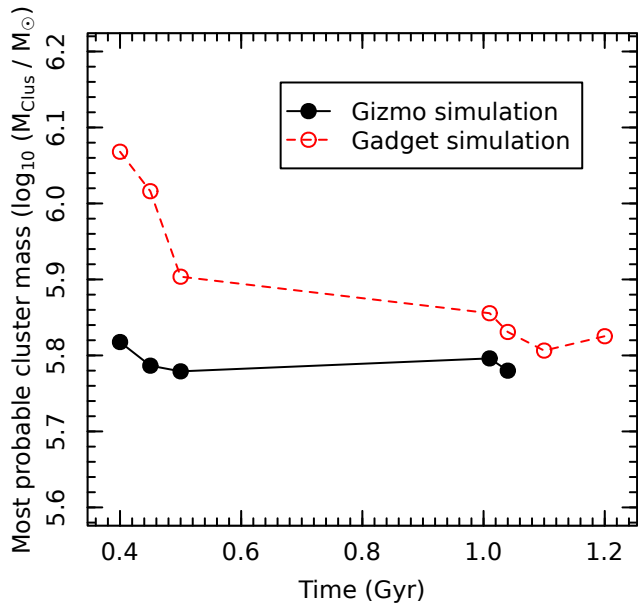


**Figure 6.** The most probable star cluster mass as a function of time from both GIZMO (black) and GADGET (red) simulations. The data points correspond to the snapshot times in Figure 5.

of more than 1 Gyr, despite the fact that a number of processes important to cluster destruction, such as tidal destruction, shock heating, and supernova explosion, are included in the hydrodynamical simulations. These results suggest that the observed globular clusters

may form in interacting galaxies at high redshift when the merger rate was high (Rodríguez-Gomez et al. 2015; Mistani et al. 2016). The extremely high gas pressures in the merging environments produce lognormal ICMFs with a peak mass around  $\sim 10^6 M_\odot$ , and they evolve slowly over a Hubble time into the universal lognormal profiles with a peak at  $\sim 1.5 - 3 \times 10^5 M_\odot$  as observed today.

## 5. DISCUSSION

We have used the two codes GADGET and GIZMO with significantly different hydrodynamical solvers to simulate the formation and evolution of SCs in galaxy mergers and found similar results. This helps us to reduce the possibility of significant numerical artifacts in our results and suggests that our findings are physical and robust.

In GADGET, the hydrodynamic solver uses a smoothing scheme (Springel 2005), where the physical properties are averaged over a given number of neighboring particles, which is 32 in our simulation. The mass of 32 star particles for our resolution is close to the peak cluster mass seen in the GADGET simulation. However, the GIZMO simulation has no smoothing procedure and the properties do not depend on the number of neighbors but we still see the cluster mass peak at similar masses. This suggests that the peak cluster mass found in our simulation is likely not a numerical artifact, but rather may be a physical feature of SCs formed in such extreme environments. One very potent source of the

high pressure in our simulations is the shocks produced during the close passages of galaxies and starburst periods. GIZMO handles shocks much better than GADGET, and it calculates the effects of contact discontinuities more precisely, captures fluid mixing instabilities well and has less numerical noise. These differences are pronounced in Figure 4, where the pressure distribution is more cleanly peaked in GIZMO whereas it is quite spread out in GADGET.

We have seen from Figure 3 that the ICMF in our simulations does not have the shape of a falling power law, which is commonly observed for many YMC systems. Rather, the ICMF has a quasi-lognormal shape which is preserved in later stages. We doubt that this is due to the limited mass resolution ( $5 \times 10^4 M_\odot$ ) in our simulations, as similar ICMFs were also reported by Renaud et al. (2015), who performed a simulation of the Antennae using a grid-based AMR code with very high mass resolution ( $\sim 70 M_\odot$ ). The agreement among the merger simulations using different codes, various feedback prescriptions and across resolution suggest that the lognormal-shape ICMFs and the unique mass peak are mostly likely special features of clusters formed in the extremely high pressure environments produced by galaxy collisions. In fact, some studies of active galaxies, such as the starburst galaxy NGC 5253 (Cresci et al. 2005) and the interacting Antennae pair (Anders et al. 2007) have shown that the ICMF for YMCs is not a power law for all mass scales, but may rather have a turnover at low mass.

As indicated by Figure 5 and Figure 6, over the evolution of more than 1 Gyr, the mass functions of our star clusters in both the GADGET and GIZMO simulations survives destructive processes and retain the same quasi-lognormal shape with a consistent peak at around  $\sim 10^{5.8} M_\odot$ . This mass is quite close to the observed GCMF peak at  $\sim 1.5 - 3 \times 10^5 M_\odot$ . Ideally we would like to have a fully cosmological hydrodynamic simulation of galaxy formation and evolution with a very high mass resolution ( $\sim 10^3 M_\odot$ ) to identify SCs and evolve them for  $\sim 13$  Gyr to explore the fate of the globular cluster mass function, but that remains computationally very expensive. However, the strong trend of survival of the lognormal shape of the ICMFs in our simulations lends support to our speculation that the origin of the lognormal mass functions of the globular clusters may come from the extremely high pressure formation conditions in interacting galaxies.

## 6. CONCLUSIONS

We have performed high-resolution hydrodynamic simulations of galaxy mergers using two different codes and studied the formation and evolution of SCs in them. We obtained consistent results from both codes, suggest-

ing that our results are physical and robust. Here is a summary of our findings:

- A strong galaxy interaction produces intense shocks and compression of gas, which triggers global starbursts and the formation of massive SCs in the nuclear regions of the mergers and in the tidal bridges and tails. The massive star clusters show quasi-lognormal ICMFs in the range of  $\sim 10^{5.5-7.5} M_\odot$  with a peak around  $10^6 M_\odot$ .
- The nascent cluster-forming gas clouds have very high pressures in the range of  $P/k \sim 10^{8-12} \text{ K cm}^{-3}$ , in good agreement with observations and theoretical expectations that massive SCs form in high-pressure environments, which naturally arise in violent galaxy collisions. Moreover, the gas pressures show quasi-lognormal profiles, which suggests that the quasi-lognormal ICMFs of the clusters may be caused by the pressure distributions in the birth clouds. Furthermore, the peak of the pressure distribution correlates with the peak of the cluster mass function at  $10^{5.8-6.2} M_\odot$ , indicating that clusters formed in such extremely high pressure clouds have a characteristic mass around  $\sim 10^6 M_\odot$ .
- The cluster mass functions evolve slowly over time with a declining cluster number due to destructive processes, but the quasi-lognormal shape and the peak of the mass functions do not change significantly during the course of galaxy collisions over 1 Gyr.

Our results suggest that the observed universal lognormal globular cluster mass functions and the unique peak at  $\sim 2 \times 10^5 M_\odot$  may originate from the high-pressure formation conditions in the birth clouds. Globular clusters may have formed in extremely high pressure environments produced by violent galaxy interactions at high redshift when mergers were more common. The lognormal cluster mass functions with a preferred most probable cluster mass around  $\sim 10^6 M_\odot$  may be unique products of such extreme birth conditions, and they evolve slowly over 13 Gyrs but retain the lognormal shape and peak against destructive processes.

## ACKNOWLEDGEMENT

We thank Dr. Bruce Elmegreen and Dr. Phil Hopkins for valuable discussions that have improved the project. YL acknowledges support from NSF grants AST-0965694, AST-1009867 and AST-1412719. AK is supported by the *Ministerio de Economía y Competitividad* (MINECO) in Spain through grants AYA2012-31101 and AYA2015-63810-P as well as the Consolider-Ingenuo 2010 Programme of the *Spanish Ministerio de*

*Ciencia e Innovación* (MICINN) under grant Multi-Dark CSD2009-00064. He also acknowledges support from the *Australian Research Council* (ARC) grant DP140100198. We acknowledge the Institute For Cyber-Science at The Pennsylvania State University for pro-

viding computational resources and services that have contributed to the research results reported in this paper. The Institute for Gravitation and the Cosmos is supported by the Eberly College of Science and the Office of the Senior Vice President for Research at the Pennsylvania State University.

## REFERENCES

- Adamo, A., Kruijssen, J. M. D., Bastian, N., Silva-Villa, E., & Ryon, J. 2015, *MNRAS*, 452, 246
- Agertz, O., Moore, B., Stadel, J., Potter, D., Miniati, F., Read, J., Mayer, L., Gawryszczak, A., Kravtsov, A., Nordlund, Å., Pearce, F., Quilis, V., Rudd, D., Springel, V., Stone, J., Tasker, E., Teyssier, R., Wadsley, J., & Walder, R. 2007, *MNRAS*, 380, 963
- Anders, P., Bissantz, N., Boysen, L., de Grijs, R., & Fritze-v. Alvensleben, U. 2007, *MNRAS*, 377, 91
- Annibali, F., Tosi, M., Aloisi, A., & van der Marel, R. P. 2011, *AJ*, 142, 129
- Ashman, K. M., & Zepf, S. E. 2001, *AJ*, 122, 1888
- Barnes, J. E., & Hernquist, L. 1992, *Nature*, 360, 715
- . 1996, *ApJ*, 471, 115
- Barnes, J. E., & Hernquist, L. E. 1991, *ApJL*, 370, L65
- Bastian, N. 2008, *MNRAS*, 390, 759
- Bastian, N., Hempel, M., Kissler-Patig, M., Homeier, N. L., & Trancho, G. 2005, *A&A*, 435, 65
- Bauer, A., & Springel, V. 2012, *MNRAS*, 423, 2558
- Baumgardt, H. 1998, *A&A*, 330
- Baumgardt, H., & Makino, J. 2003, *MNRAS*, 340, 227
- Bertschinger, E., & Gelb, J. M. 1991, *Computers in Physics*, 5, 164
- Bik, A., Lamers, H. J. G. L. M., Bastian, N., Panagia, N., & Romaniello, M. 2003, *A&A*, 397, 473
- Boulares, A., & Cox, D. P. 1990, *ApJ*, 365, 544
- Brodie, J. P., & Strader, J. 2006, *ARA&A*, 44, 193
- Combes, F., Leon, S., & Meylan, G. 1999, *A&A*, 352, 149
- Cox, T. J., & Loeb, A. 2008, *MNRAS*, 386, 461
- Cresci, G., Vanzi, L., & Sauvage, M. 2005, *A&A*, 433, 447
- Davis, M., Efstathiou, G., Frenk, C. S., & White, S. D. M. 1985, *ApJ*, 292, 371
- de Grijs, R. 2007, *ArXiv e-prints*
- Elmegreen, B. G. 1989, *ApJ*, 338, 178
- Elmegreen, B. G., & Efremov, Y. N. 1997, *ApJ*, 480, 235
- Fall, S. M., & Chandar, R. 2012, *ApJ*, 752, 96
- Fall, S. M., & Rees, M. J. 1985, *ApJ*, 298, 18
- Fall, S. M., & Zhang, Q. 2001, *ApJ*, 561, 751
- Feng, Y., Croft, R. A. C., Di Matteo, T., & Khandai, N. 2013, *MNRAS*, 429, 1554
- Forbes, D. A., & Bridges, T. 2010, *MNRAS*, 404, 1203
- Gieles, M., & Baumgardt, H. 2008, *MNRAS*, 389, L28
- Gill, S. P. D., Knebe, A., & Gibson, B. K. 2004, *MNRAS*, 351, 399
- Gingold, R. A., & Monaghan, J. J. 1977, *MNRAS*, 181, 375
- Gnedin, O. Y., Hernquist, L., & Ostriker, J. P. 1999a, *ApJ*, 514, 109
- Gnedin, O. Y., Lee, H. M., & Ostriker, J. P. 1999b, *ApJ*, 522, 935
- Gnedin, O. Y., & Ostriker, J. P. 1997, *ApJ*, 474, 223
- Goddard, Q. E., Bastian, N., & Kennicutt, R. C. 2010, *MNRAS*, 405, 857
- Gratton, R. G., Carretta, E., & Bragaglia, A. 2012, *A&A Rv*, 20, 50
- Haardt, F., & Madau, P. 1996, *ApJ*, 461, 20
- Harris, W. E. 1991, *ARA&A*, 29, 543
- Harris, W. E. 2001, in *Saas-Fee Advanced Course 28: Star Clusters*, ed. L. Labhardt & B. Binggeli, 223
- Hayward, C. C., Torrey, P., Springel, V., Hernquist, L., & Vogelsberger, M. 2014, *MNRAS*, 442, 1992
- Hernquist, L. 1990, *ApJ*, 356, 359
- Hernquist, L., & Katz, N. 1989, *ApJS*, 70, 419
- Herrera, C. N., Boulanger, F., & Nesvadba, N. P. H. 2011, *A&A*, 534, A138
- Holtzman, J. A., Faber, S. M., Shaya, E. J., Lauer, T. R., Groth, J., Hunter, D. A., Baum, W. A., Ewald, S. P., Hester, J. J., Light, R. M., Lynds, C. R., O’Neil, Jr., E. J., & Westphal, J. A. 1992, *AJ*, 103, 691
- Hopkins, P. F. 2015, *MNRAS*, 450, 53
- Hopkins, P. F., Hernquist, L., Cox, T. J., Di Matteo, T., Martini, P., Robertson, B., & Springel, V. 2005, *ApJ*, 630, 705
- Hopkins, P. F., Hernquist, L., Cox, T. J., & Kereš, D. 2008, *ApJS*, 175, 356
- Hopkins, P. F., Hernquist, L., Cox, T. J., Robertson, B., & Springel, V. 2006, *ApJS*, 163, 50
- Jenkins, E. B., Jura, M., & Loewenstein, M. 1983, *ApJ*, 270, 88
- Jog, C. J., & Das, M. 1996, *ApJ*, 473, 797
- Jog, C. J., & Solomon, P. M. 1992, *ApJ*, 387, 152
- Johnson, K. E., Leroy, A. K., Indebetouw, R., Brogan, C. L., Whitmore, B. C., Hibbard, J., Sheth, K., & Evans, A. S. 2015, *ApJ*, 806, 35
- Jordán, A., McLaughlin, D. E., Côté, P., Ferrarese, L., Peng, E. W., Mei, S., Villegas, D., Merritt, D., Tonry, J. L., & West, M. J. 2007, *ApJS*, 171, 101
- Kennicutt, Jr., R. C. 1998, *ApJ*, 498, 541
- Kereš, D., Vogelsberger, M., Sijacki, D., Springel, V., & Hernquist, L. 2012, *MNRAS*, 425, 2027
- Keto, E., Ho, L. C., & Lo, K.-Y. 2005, *ApJ*, 635, 1062
- Klypin, A., & Holtzman, J. 1997, *ArXiv Astrophysics e-prints*
- Knierman, K. A., Gallagher, S. C., Charlton, J. C., Hunsberger, S. D., Whitmore, B., Kundu, A., Hibbard, J. E., & Zaritsky, D. 2003, *AJ*, 126, 1227
- Knollmann, S. R., & Knebe, A. 2009, *ApJS*, 182, 608
- Kruijssen, J. M. D. 2014, *Classical and Quantum Gravity*, 31, 244006
- . 2015, *MNRAS*, 454, 1658
- Kruijssen, J. M. D., & Cooper, A. P. 2012, *MNRAS*, 420, 340
- Kruijssen, J. M. D., Pelupessy, F. I., Lamers, H. J. G. L. M., Portegies Zwart, S. F., Bastian, N., & Icke, V. 2012, *MNRAS*, 421, 1927
- Kruijssen, J. M. D., Pelupessy, F. I., Lamers, H. J. G. L. M., Portegies Zwart, S. F., & Icke, V. 2011, *MNRAS*, 414, 1339
- Lamers, H. J. G. L. M., Baumgardt, H., & Gieles, M. 2010, *MNRAS*, 409, 305
- Larsen, S. S. 2010, *Philosophical Transactions of the Royal Society of London Series A*, 368, 867
- Li, Y., Hernquist, L., Robertson, B., Cox, T. J., Hopkins, P. F., Springel, V., Gao, L., Di Matteo, T., Zentner, A. R., Jenkins, A., & Yoshida, N. 2007, *ApJ*, 665, 187
- Li, Y., Mac Low, M.-M., & Klessen, R. S. 2004, *ApJL*, 614, L29

- Longmore, S. N., Kruijssen, J. M. D., Bastian, N., Bally, J., Rathborne, J., Testi, L., Stolte, A., Dale, J., Bressert, E., & Alves, J. 2014, *Protostars and Planets VI*, 291
- Lützgendorf, N., Baumgardt, H., & Kruijssen, J. M. D. 2013, *A&A*, 558, A117
- McCrary, N., & Graham, J. R. 2007, *ApJ*, 663, 844
- McLaughlin, D. E., & Fall, S. M. 2008, *ApJ*, 679, 1272
- Mengel, S., Lehnert, M. D., Thatte, N., & Genzel, R. 2002, *A&A*, 383, 137
- Mengel, S., Lehnert, M. D., Thatte, N. A., Vacca, W. D., Whitmore, B., & Chandar, R. 2008, *A&A*, 489, 1091
- Miah, J. A., Sharples, R. M., & Cho, J. 2015, *MNRAS*, 447, 3639
- Mihos, J. C., & Hernquist, L. 1994, *ApJL*, 431, L9
- . 1996, *ApJ*, 464, 641
- Miller, B. W., Whitmore, B. C., Schweizer, F., & Fall, S. M. 1997, *AJ*, 114, 2381
- Mistani, P. A., Sales, L. V., Pillepich, A., Sanchez-Janssen, R., Vogelsberger, M., Nelson, D., Rodriguez-Gomez, V., Torrey, P., & Hernquist, L. 2016, *MNRAS*, 455, 2323
- Mo, H. J., Mao, S., & White, S. D. M. 1998, *MNRAS*, 295, 319
- Mullan, B., Konstantopoulos, I. S., Kepley, A. A., Lee, K. H., Charlton, J. C., Knierman, K., Bastian, N., Chandar, R., Durrell, P. R., Elmegreen, D., English, J., Gallagher, S. C., Gronwall, C., Hibbard, J. E., Hunsberger, S., Johnson, K. E., Maybhate, A., Palma, C., Trancho, G., & Vacca, W. D. 2011, *ApJ*, 731, 93
- Nelson, D., Vogelsberger, M., Genel, S., Sijacki, D., Kereš, D., Springel, V., & Hernquist, L. 2013, *MNRAS*, 429, 3353
- Parmentier, G., & Gilmore, G. 2007, *MNRAS*, 377, 352
- Portegies Zwart, S. F., McMillan, S. L. W., & Gieles, M. 2010, *ARA&A*, 48, 431
- Prieto, J. L., & Gnedin, O. Y. 2008, *ApJ*, 689, 919
- Renaud, F., Bournaud, F., & Duc, P.-A. 2015, *MNRAS*, 446, 2038
- Renaud, F., & Gieles, M. 2013, *MNRAS*, 431, L83
- Renaud, F., Gieles, M., & Boily, C. M. 2011, *MNRAS*, 418, 759
- Rodriguez-Gomez, V., Genel, S., Vogelsberger, M., Sijacki, D., Pillepich, A., Sales, L. V., Torrey, P., Snyder, G., Nelson, D., Springel, V., Ma, C.-P., & Hernquist, L. 2015, *MNRAS*, 449, 49
- Schaye, J., Crain, R. A., Bower, R. G., Furlong, M., Schaller, M., Theuns, T., Dalla Vecchia, C., Frenk, C. S., McCarthy, I. G., Helly, J. C., Jenkins, A., Rosas-Guevara, Y. M., White, S. D. M., Baes, M., Booth, C. M., Camps, P., Navarro, J. F., Qu, Y., Rahmati, A., Sawala, T., Thomas, P. A., & Trayford, J. 2015, *MNRAS*, 446, 521
- Schmidt, M. 1959, *ApJ*, 129, 243
- Schweizer, F., Miller, B. W., Whitmore, B. C., & Fall, S. M. 1996, *AJ*, 112, 1839
- Sijacki, D., Vogelsberger, M., Kereš, D., Springel, V., & Hernquist, L. 2012, *MNRAS*, 424, 2999
- Springel, V. 2000, *MNRAS*, 312, 859
- . 2005, *MNRAS*, 364, 1105
- Springel, V., Di Matteo, T., & Hernquist, L. 2005a, *MNRAS*, 361, 776
- Springel, V., & Hernquist, L. 2002, *MNRAS*, 333, 649
- . 2003a, *MNRAS*, 339, 289
- . 2003b, *MNRAS*, 339, 312
- . 2005, *ApJL*, 622, L9
- Springel, V., White, S. D. M., Jenkins, A., Frenk, C. S., Yoshida, N., Gao, L., Navarro, J., Thacker, R., Croton, D., Helly, J., Peacock, J. A., Cole, S., Thomas, P., Couchman, H., Evrard, A., Colberg, J., & Pearce, F. 2005b, *Nature*, 435, 629
- Springel, V., Yoshida, N., & White, S. D. M. 2001, *NewA*, 6, 79
- Suginohara, T., & Suto, Y. 1992, *ApJ*, 387, 431
- VandenBerg, D. A., Brogaard, K., Leaman, R., & Casagrande, L. 2013, *ApJ*, 775, 134
- Vesperini, E. 2000, *MNRAS*, 318, 841
- . 2001, *MNRAS*, 322, 247
- Vesperini, E., & Heggie, D. C. 1997, *MNRAS*, 289, 898
- Vogelsberger, M., Sijacki, D., Kereš, D., Springel, V., & Hernquist, L. 2012, *MNRAS*, 425, 3024
- Warren, M. S., Quinn, P. J., Salmon, J. K., & Zurek, W. H. 1992, *ApJ*, 399, 405
- Webb, J. J., & Leigh, N. W. C. 2015, *MNRAS*, 453, 3278
- Wei, L. H., Keto, E., & Ho, L. C. 2012, *ApJ*, 750, 136
- Welty, D. E., Lauroesch, J. T., Wong, T., & York, D. G. 2016, *ApJ*, 821, 118
- Whitmore, B. C., Chandar, R., Schweizer, F., Rothberg, B., Leitherer, C., Rieke, M., Rieke, G., Blair, W. P., Mengel, S., & Alonso-Herrero, A. 2010, *AJ*, 140, 75
- Whitmore, B. C., & Schweizer, F. 1995, *AJ*, 109, 960
- Whitmore, B. C., Schweizer, F., Leitherer, C., Borne, K., & Robert, C. 1993, *AJ*, 106, 1354
- Whitmore, B. C., Zhang, Q., Leitherer, C., Fall, S. M., Schweizer, F., & Miller, B. W. 1999, *AJ*, 118, 1551
- Zhang, H.-X., Gao, Y., & Kong, X. 2010, *MNRAS*, 401, 1839
- Zhang, Q., & Fall, S. M. 1999, *ApJL*, 527, L81
- Zhu, Q., Hernquist, L., & Li, Y. 2015, *ApJ*, 800, 6
- Zhu, Q., & Li, Y. 2016, *ArXiv* 1606.00796
- Zubovas, K., Sabulis, K., & Naujalis, R. 2014, *MNRAS*, 442, 2837